Journal of
Water & Climate Change

IWA PUBLISHING

Journal of Water and Climate Change Vol 13 No 2, 839 doi: 10.2166/wcc.2021.348

Temporal change of extreme precipitation intensity–duration–frequency relationships in Thailand

N. Yamoat[a,*], R. Hanchoowong[b], S. Sriboonlue[c] and A. Kangrang[d]

[a] Department of Civil and Environmental Engineering Technology, King Mongkut's University of Technology North Bangkok, 1518 Pracharat 1 Road, Wongsawang, Bangsue, Bangkok 10800, Thailand
[b] Department of Civil Engineering, Mahanakorn University of Technology, 140 Cheum-Sampan Road, Nong Chok, Bangkok 10530, Thailand
[c] Arcadis U.S., Suite 200, Irvine, CA 92602, USA
[d] Faculty of Engineering, Mahasarakham University, Khamriang, Kantarawichai, Maha Sarakham 44150, Thailand
*Corresponding author. E-mail: nirat.y@cit.kmutnb.ac.th

SS, 0000-0002-4927-5326; AK, 0000-0003-2575-264X

ABSTRACT

Due to climate change, many research studies have derived the updated extreme precipitation intensity–duration–frequency relationship (IDF curve) from forecasted sub-hourly rainfall intensity time series, which is one of the most important tools for the planning and designing of hydraulic infrastructures. In this study, the IDF curves (1990–2016) of the six regions and procedures are used in accordance with those of the Royal Irrigation Department (RID)'s study (1950–1988). Each set of IDF relationships consists of 81 intensity values which are the combination of nine durations and nine return periods. The intensity ratios of this study and RID are compared. A greater-than-1 ratio indicates extreme intensity increment from the past to the present. Considering 81 ratios for each region, the number of greater-than-1 ratios for the North, Northeast, Central, East, West, and South regions are 8, 2, 31, 34, 6, and 7, respectively. These ratio numbers are far below 81 which means that the majority of extreme rainfall intensities do not increase from the past to the present. The study found that using accurate historical sub-hourly rainfall time series to create a set of IDF curves would be more reliable than using forecasted rainfall modeling.

Key words: extreme precipitation intensity, IDF relationship, temporal change, Thailand

HIGHLIGHTS

- Using accurate historical sub-hourly rainfall time series to create a set of IDF curves would be more reliable than using forecasted rainfall modeling.
- The future period intensities from eight global climate models are closer to the base period intensities than the ones from a global climate model.
- The majority of recent and past IDF curves did not increase as expected.

INTRODUCTION

Expected rainfall intensity is required and used in the planning and design of engineering and environmental infrastructures in that it is termed the design storm (Balbastre-Soldevila *et al.* 2019; Cook *et al.* 2020). The appropriate design storm must be neither too large nor too small. When too large, the concerned infrastructure will be unnecessarily overdesigned and expensive, while when too small it will risk the damage caused by flood or heavy rain. A suitable design storm can be estimated from the relationship of extreme rainfall intensity, its duration, and frequency of occurrence. Generally, the shorter duration of the storm, the heavier the rainfall. Also, the heavier the storm, the less frequently it occurs. The imperative tool for planners and engineers to choose the appropriate design storm is, therefore, an accurate maximum rainfall intensity–duration–frequency (IDF) relationship (Mirhosseini *et al.* 2012; Sun *et al.* 2019). It is actually the relationship of the maximum rainfall intensity (or depth) at a specific duration and a specific return period. It can be in the form of the table of maximum intensity values at several durations and return periods or a set of curves of maximum intensity as a function of duration at several return periods, a so-called IDF curve. A return period is an average length of time that a specified, or higher, rainfall intensity occurs at a particular place with a specified duration.

An IDF curve was initiated by Sherman (1931) and Bernard (1932) and since then it has been extensively used in the USA (Hershfield 1962) and is spreading worldwide (Bezak *et al.* 2018). In Thailand, Mustonen (1969) originally proposed 14 curves, i.e., five curves for the Northeast, two each for the Northern, Central, Eastern, and Southern regions, and just one curve for the West. The Royal Irrigation Department (RID), the main responsible institute for irrigation and drainage in Thailand, issued a detailed study of IDF curves and specified a total of 59 curves for the whole country. They are 20 for the North, 10 for the Northeast, 5, 8, 4, and 12 for the Central, East, West, and South, respectively (Bumpenkit 1999). The average representative IDF curves for each of the five regions were also presented.

An IDF relationship is usually derived from historical data of sub-hourly rainfall intensity time series, usually 15 min in Thailand, for many years of records (Bumpenkit 1999; Shrestha *et al.* 2017). Annual maximum intensity values at each of several durations, e.g., 0.25, 0.5, 0.75, 1, 2, 3, 6, 12, and 24 h are extracted from the time series and then being used for constructing IDF curves (Koutsoyiannis *et al.* 1998). After the last few decades, Thailand as well as other countries experienced flooding more frequently in both urban and rural areas and climate change was thought to be one of the causes (Shrestha *et al.* 2017; Choi *et al.* 2019). It has been suspected that the official IDF curves for each country might be underestimated for the designed storms that cause more frequent flooding due to the global warming. Climate change with the increase of greenhouse gas is however expected to result in higher maximum rainfall intensity in the future, since a warmer atmosphere raises its water holding capacity by 7% for every 1% of rising temperature (Trenberth 2011; Cheng & AghaKouchak 2014; Ganguli & Coulibaly 2017). The earth's mean temperature has been rising for 1.2–1.5 °C since a the pre-industrialized period (Hu & Ayub 2019; Jacobson *et al.* 2019). This impelled a lot of researchers to create new sets of IDF curves in parallel with future rainfall data which are not real and not yet existing (Noor *et al.* 2018). Thus, we should create the most accurate and precise future rainfall data from the global climate modeling (GCM).

Future rainfall data can be created via GCM or regional climate modeling (RCM) (Agilan & Umamahesh 2016; Kohnova *et al.* 2019). Both types of models are similar in all aspects except that the global models cover or nearly cover the whole world, while the regional models involve only portions of the earth. An RCM is always derived from a GCM to be able to apply for an area of interest. Several institutes produced future climate data either from GCMs or RCMs depending on their interest (Moriondo & Bindi 2006; Chokkavarapu & Mandla 2019). They simulate the interaction of atmosphere, ocean, land, and sea ice, which are changing all the time. Only transient GCMs (not the steady state ones) can forecast the future climate data of which only precipitation is of interest to this study (White *et al.* 2009). GCMs are make of numerical methods to solve the equations of conservations of mass, energy, and momentum with three-dimensional grids and a regular time step. A historical global gridded precipitation data set is needed for appropriate initial and boundary conditions and bias correction.

A daily time step is usually the highest temporal resolution obtained from GCM simulations; however, to produce IDF relationships, a higher resolution of 15 min or less is needed. Therefore, a procedure to disaggregate the daily to 15 min time step is need (Sun *et al.* 2019). The highest spatial resolution is normally about $1° \times 1°$ lat/lon, about 100 km, which is too large and needs to be downscaled (Wilby *et al.* 2002; Cook *et al.* 2020). Having obtained 15-min rainfall intensity time series, the annual maximum series of rainfall intensity for several durations up to 24 or 48 h can be derived. For this derivation, we always assume that the annual maximum series data are stationary, meaning that the statistics of the data are temporally constant. Naturally, it is not so, therefore, nonstationary annual maximum series of rainfall intensity in the future are to be assumed. The future rainfall data of annual maximum series must be created in order to derive an accurate IDF curve (AghaKouchak *et al.* 2018; Ganguli & Coulibaly 2019). Furthermore, we must estimate the future atmospheric composition scenarios from very low greenhouse gas emission or concentration to very high.

The lengthy procedure for the future IDF curve modeling makes their accuracy and precision skeptical (Bellprat *et al.* 2019; Thompson & Smith 2019; Buchanan 2020; Cook *et al.* 2020). Each step of calculation produces errors and uncertainties which can add up tremendously. Can we be confident that the derived sets of maximum rainfall are accurate and precise? The accuracy of a current IDF relationship would not be known beforehand let alone that of the future IDF. This is because the predicted values of maximum rainfall intensity are not the actual values which have not yet existed at the time of the infrastructure being designed. For example, the value of a rainfall intensity at a 25-year return period means that the actual value will be known at least in 25 years to come or even 100 years or more. A majority of previous research found that the return levels for future IDF curves were always higher than the present ones (Liew *et al.* 2013). Shrestha *et al.* (2017), for example, created the IDF curves of periods 20112030 and 20462065 for Bangkok, the capital city of Thailand. They found that most of the future return levels are larger than that of the present ones. As aforementioned, the lengthy procedure of future IDF curve productions involves numerous assumptions, approximations, and uncertainties that they cannot be trusted. Several

researchers recently have tried to use the reliable past data to predict future extreme events (Shepherd *et al.* 2018; Woo & Johnson 2018; Sillmann *et al.* 2021; and references therein). However, they are still not accurate and precise enough. This study attempts to derive new sets of IDF curves for all regions of Thailand (data periods: 1990–2016) and compares them to those of the original Royal Irrigation Department (1950–1998) using exactly the same methodology. The number of stations and their record lengths may not be the same for each pair of corresponding regions but average values will be used for comparison.

The aim of the study is, therefore, to compare the IDF relationships of the current study to those of the national standard in Bumpenkit (1999) to quantify the change of extreme rainfall intensities of the two periods to determine the acceptability of the official IDF curves.

STUDY AREA

Thailand is a part of mainland Southeast Asia situated between 97.1–106.0 E and 5.4–20.6 N and surrounded by Myanmar, Laos, Cambodia, and Malaysia. It is divided into six regions, namely Northern, Northeastern, Central, Western, Eastern, and Southern (Figure 1(a)). A series of mountain ranges run in the north-south direction extending from the Northern region passing the Western to the Southern one, these mountain ranges are on the west and border Thailand with Myanmar (Figure 1(b)). The trans-boundary Mekong River that runs along the eastern boundary divides Thailand from Lao and Cambodia. The Northeast region is a plateau with the Mekong on to the east. The Central region is a lowland receiving flood flow

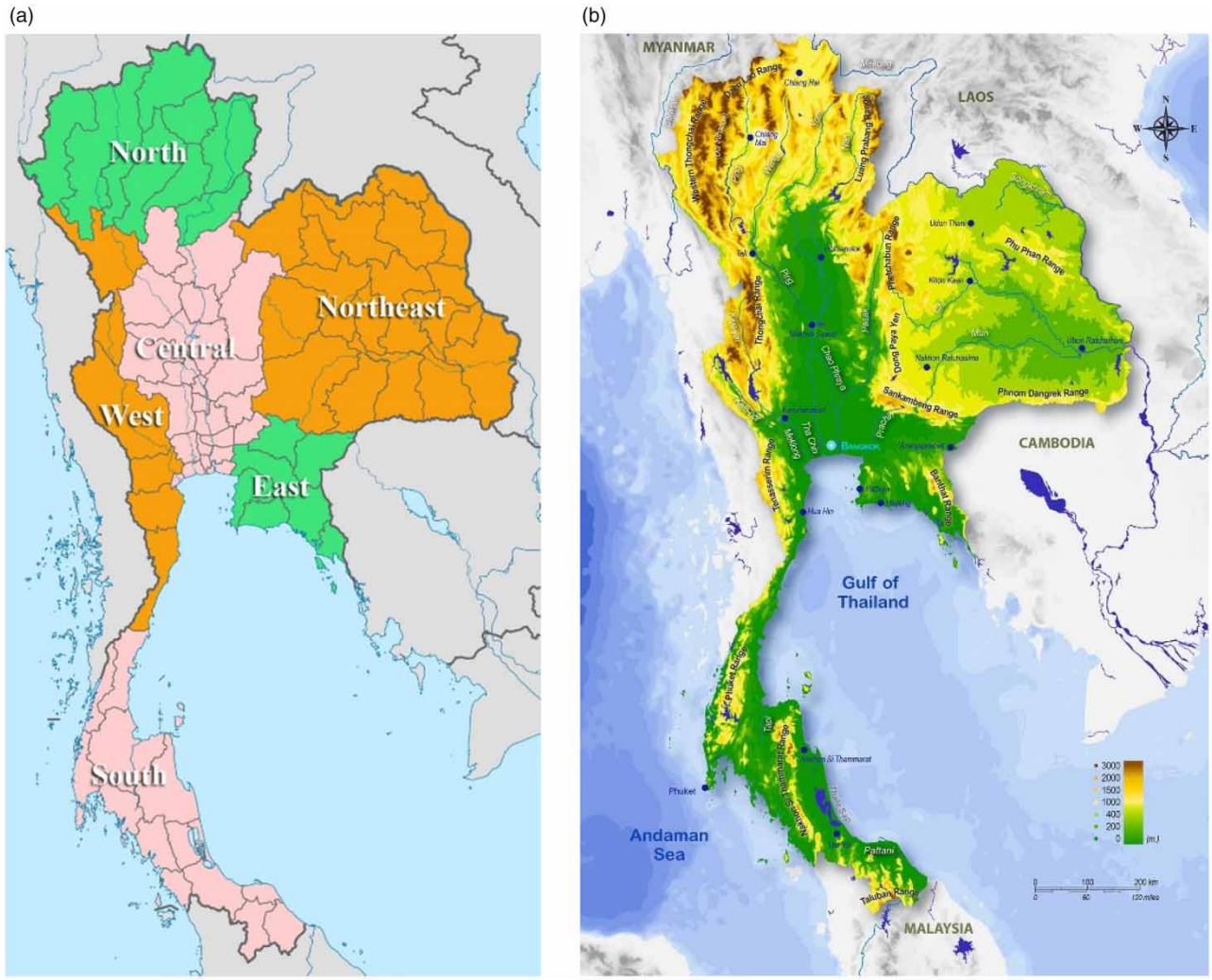

Figure 1 | Six geoclimatic regions of Thailand: (a) regions and (b) geography (Martin & Riichie 2020).

from the North and draining to the Gulf of Thailand. The Central normally includes the western and eastern regions; however, since their precipitation characteristics are different, we separate them for the purposes of this study. The Southern region of Thailand is a peninsula extending southward from the Central region to Malaysia with the Gulf of Thailand (of Pacific Ocean) on the east and Andaman Sea (of Indian Ocean) on the west. (Figure 1(b)).

The climate characteristics of Thailand are governed by the dynamics of the Intertropical Convergence Zone (ITCZ), a low atmospheric pressure band occurring from the combination of the solar radiation intensity and the inclination of the earth axis. During a few months at the beginning of the year, the ITCZ is located far below Malaysia; therefore, Thailand is without rainfall. The ITCZ moves rapidly northward to the western, central, and eastern parts in May and slowly moving to the north passing the Central, Northeastern, and Northern departing the northern boundary in mid-July. During the period of the ITCZ passing, it induces humidity from the Indian Ocean and the Gulf of Thailand, as southwest monsoon, to the upper part of the country. After a few weeks, the ITCZ comes back from China to the northern part of Thailand again, leaving the country's upper part to the south in mid-October. From July to October, the humidity from the southwest monsoon from the Indian Ocean plus the tropical cyclone from the South China Sea and the Pacific Ocean moves to Thailand's upper part creating heavy rainfall. After departing the upper part, the ITCZ moves across the peninsula from October to the New Year causing heavy rain in the Southern region. Accordingly, precipitation patterns of Thailand can be separated into two main regions: the upper and lower parts. The upper includes the Northern, Western, Northeastern, Central, and Eastern regions, whereas the lower is the Southern region. The lower part consists of two seasons, that is, the dry season from January to April and the rainy season from May to December. The upper part has three seasons: summer from February to April, rainy season from May to October, and cool season from November to January. The rainy season can also be separated into two periods by a drought spell: the former rainy season from May to July and the latter rainy season with a higher peak from August to October.

METHODS

The maximum rainfall IDF relationship (IDF curve) of a homogeneous region is always presented as a set of curves of maximum average intensity as a function of duration in that each curve has a fixed return period. To create the relationship, the data of annual maximum rainfall intensities at several corresponding durations of rain from several automatic rain gauges are required. For example, for 20 years of data from a rainfall station, there are 20 maximum intensity values for each of a number of durations, i.e., 15, 30, 45 min, 1 h, 2, 3, 6, 12, and 24 h in this study. An automatic rain gauge usually gives a time series of rainfall depths of a given temporal resolution, e.g. 15 min, which is common in Thailand, for each year. These rainfall depth time series are divided by the time resolution to obtain the time series of average rainfall intensities. The maximum average intensity of each year for each of the nine durations has to be evaluated. Let $\xi_{15}(t)$ be a time series of average rainfall intensities for the 15-min resolution from the beginning to the end of a year; therefore, the maximum average intensity, $i(15)$, of the year is as follows:

$$i(15) = \max\{\xi_{15}(t)\},\ \ t = 15, 30, 45\,\text{min},\ \ldots \tag{1}$$

where t is the resolution time step. The time series of average rainfall intensities for the durations, d, other than 15 min, which are integer multiples, N, of the resolution, can be calculated from the following equation (Koutsoyiannis *et al.* 1998):

$$\xi_d\ = \frac{d\sum \xi_\delta(t - i\delta)}{d} \tag{2}$$

where δ is the resolution duration which is 15 min in this study, the summation is from $i = 0$ to $N - 1$, and N is an integer multiple of the resolution. Then the maximum intensity for durations other than 15 min can be evaluated from the time series $\xi_d(t)$ of a year as:

$$i(d) = \max\{\xi_d(t)\} \tag{3}$$

The procedures described in Equations (1)–(3) are applied to the time series of average rainfall intensities of 15 min resolutions for all annual data sets. Then for each of the rainfall stations, there are nine sets of annual maximum rainfall intensity series, denoted by i_{15}, i_{30}, i_{45}, …, i_{24} for the durations of 15, 30, 45 min, …., 24 h, respectively.

Each set of annual maximum rainfall intensities was assumed to follow the distribution of the extreme value type I (EV I) or Gumbel distribution which is the popular one for extrapolating to higher return levels (Koutsoyiannis *et al.* 1998; da Silva *et al.* 2019). To model the EV I distribution, we need two parameters, namely location parameter, u, and scale parameter, β, which can be evaluated using the method of moment as follows (Chow *et al.* 1988):

$$u = \mu - 0.5772\beta \tag{4}$$

$$\beta = \sqrt{6}\frac{\sigma}{\pi} \tag{5}$$

where μ and σ are the mean and standard deviations of the annual maximum intensity series. From the cumulative distribution function of the EV I model, for each fixed rain duration, the return level or corresponding intensity, i, can be evaluated from the following equation (Chow *et al.* 1988),

$$i = u - \beta \ln\left[\ln\left(\frac{T}{(T-1)}\right)\right] \tag{6}$$

where T is the return period. Equation (6) shows that only intensity and return period are the random variables excluding the duration.

The first step in evaluating maximum intensity $i(d,T)$ involved collecting annual intensity maxima at nine rain durations of 0.25, 0.5, 0.75, 1, 2, 3, 6, 12, and 24 h from each of automatic rain gauge stations. There are several automatic stations scattered all over Thailand and we separated them into six geoclimatic regions, namely the North (N), Northeast (Ne), Central (C), West (W), East (E), and South (S). Each region has a number of maximum intensity data of varied length as shown in Table 1 which shows that the basic data of the two studies (RID and this study) were not identical. The average and standard deviation of each data set were calculated, and then they were spatially averaged for each region (see also Figure 2).

The average values of the mean and standard deviation of each region were used to estimate the spatially average location and scale parameters from Equations (4) and (5), respectively. At each of nine rain durations, we used Equation (6) to estimate the corresponding maximum intensities of the specified return periods of 2, 5, 10, 25, 50, 100, 200, 500, and 1,000 years for each region.

RESULTS AND DISCUSSION

The derivation results of IDF relationships of this study are presented and then they were shown against the study of RID. Lastly, the ratios of the corresponding maximum intensities of this study to those of the RID were presented and discussed.

Table 1 | Basic information from the RID study (Bumpenkit 1999) and this study

Publication	Region	Number	Latitude	Longitude	Period
RID	North	20	16.07–18.84	98.75–101.16	1953–1995
	Northeast	10	14.97–17.48	101.73–104.86	1954–1998
	Central	5	13.79–15.70	99.54–100.66	1950–1998
	East	8	12.86–13.69	100.81–102.51	1960–1998
	West	4	11.81–14.34	99.49–99.95	1959–1998
	South	12	6.42–10.49	98.31–101.83	1954–1998
This study	North	8	17.62–19.96	97.98–100.78	1990–2015
	Northeast	11	14.88–17.87	102.03–105.02	1990–2015
	Central	7	13.73–16.79	99.53–101.15	1990–2015
	East	3	12.92–13.37	100.80–100.98	1990–2008
	West	6	13.00–14.24	98.55–100.06	1990–2015
	South	14	6.42–12.59	98.25–101.82	1990–2016

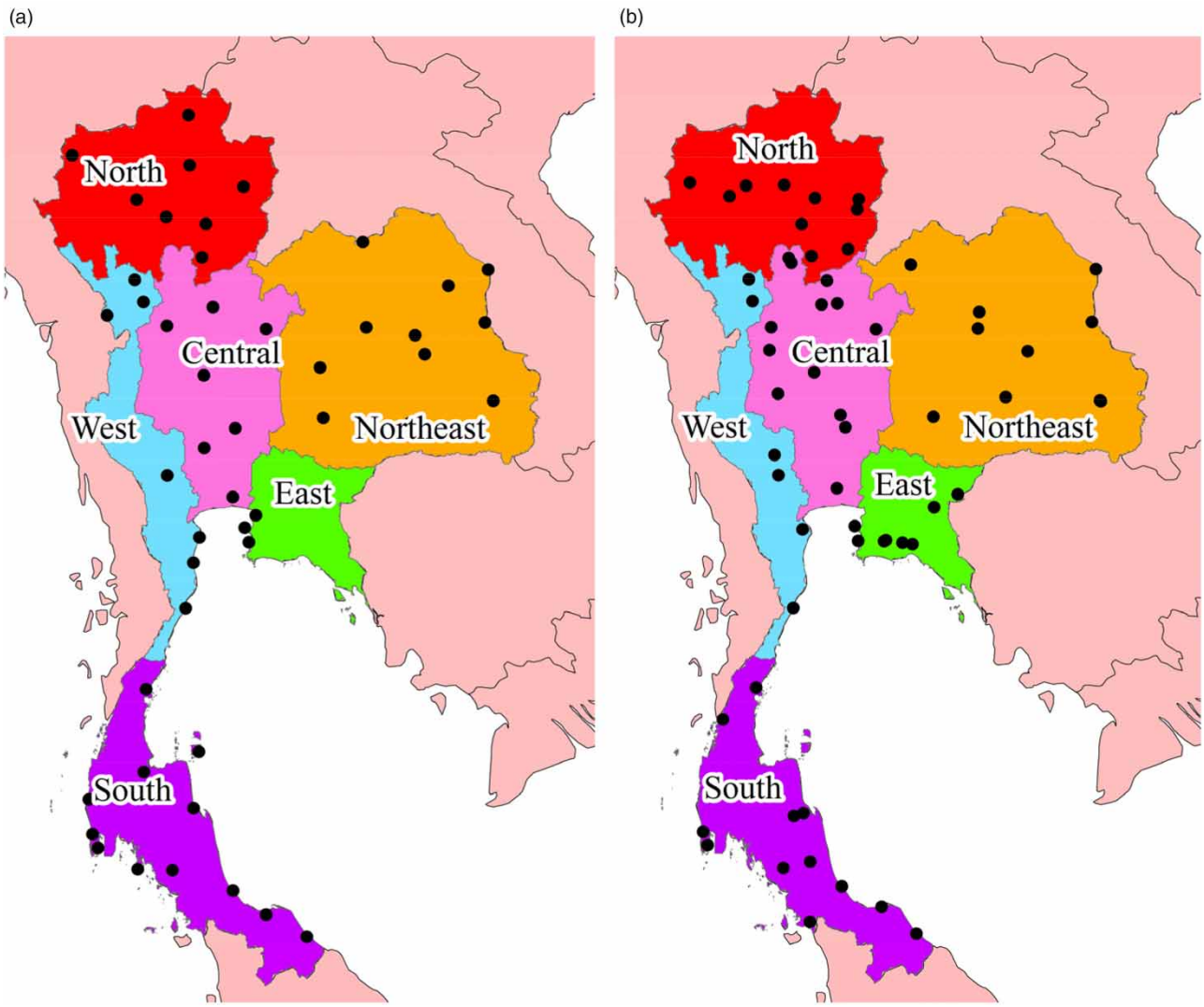

Figure 2 | Location of the stations that are used in this study and the RID study (Bumpenkit 1999): (a) this study and (b) RID's study.

Gumbel distribution parameters

Two parameters of Gumbel distribution, namely location parameter, u, and scale parameter, β, were evaluated from the means and the standard deviations of the annual maximum intensity series of each of the durations and regions. The mean values of the maximum rainfall intensity for each of the regions and each of durations are illustrated in Table 2 in

Table 2 | Spatial average values of the mean intensities at several durations for every region

	Duration (h)								
Region	0.25	0.50	0.75	1.0	2.0	3.0	6.0	12.0	24.0
N	91.99	63.83	50.43	42.05	23.85	16.98	9.20	5.06	3.13
Ne	61.58	43.62	35.65	30.22	18.13	13.14	7.30	4.02	2.80
C	76.84	55.33	44.23	37.00	21.17	15.08	8.32	4.44	3.07
E	124.29	80.81	60.81	48.59	27.45	19.22	10.35	5.38	3.43
W	87.83	59.93	46.53	38.58	23.20	17.48	9.78	5.35	3.30
S	106.20	77.71	62.24	52.04	31.53	23.00	13.30	7.82	5.42

which the maxima in durations 15 and 30 min belong to the East region and those in higher durations are in the South. For the standard deviations, the minimum spreading values belong to the North for all durations except the smallest duration which goes to the West (Table 3). Since the β parameters vary directly with the standard deviation, its minima are the same as the minimum spreading values of σ (Tables 3 and 4). The maximum values of u parameter follow the same pattern as those of the mean values (Tables 2 and 5).

IDF relationship comparison

In this subsection, we present IDF relationships from our study for all regions in Table 6 for the benefit of those who would like to use them for determining rough design storms or further research. We also add a set of IDF relationships from the RID study (Bumpenkit 1999) for the Central region only in Table 7. The reason for presenting only a single set of IDF relationships of RID is because one can determine the rest from the ratios in the next subsection. For a brief overview, the study presents only a single set of IDF curves of our study for the Central region in Figure 3. However, Figures 4–6 compare the Central region curves of this study to those of RID's study for the return periods of 2, 5, 10, 25, 50, 100, 200, 500 and 1,000 years.

Table 3 | Spatial average values of the standard deviations of the maximum intensities at several durations

	Duration (h)								
Region	**0.25**	**0.50**	**0.75**	**1.0**	**2.0**	**3.0**	**6.0**	**12.0**	**24.0**
N	41.48	22.49	18.45	16.40	9.14	6.66	3.59	1.94	1.18
Ne	44.58	30.43	25.27	22.16	14.04	10.47	6.01	3.33	2.02
C	52.97	36.51	29.30	24.61	13.96	10.01	5.55	3.06	1.73
E	48.22	28.25	20.86	17.65	11.10	8.66	5.15	2.75	1.33
W	36.98	25.92	20.03	17.65	11.53	9.63	6.1	3.63	2.35
S	38.46	26.01	20.83	17.81	11.84	8.67	5.87	3.64	2.26

Table 4 | Spatial average values of scale parameters, β

	Duration (h)								
Region	**0.25**	**0.50**	**0.75**	**1.0**	**2.0**	**3.0**	**6.0**	**12.0**	**24.0**
N	32.342	17.535	14.385	12.787	7.126	5.193	2.799	1.513	0.920
Ne	34.759	23.726	19.703	17.278	10.947	8.163	4.686	2.596	1.575
C	41.301	28.467	22.845	19.188	10.885	7.805	4.327	2.386	1.349
E	37.597	22.026	16.264	13.762	8.655	6.752	4.015	2.144	1.037
W	28.833	20.210	15.617	13.762	8.990	7.508	4.795	2.830	1.832
S	30.011	20.280	16.241	13.886	9.232	6.760	4.577	2.838	1.762

Table 5 | Spatial average values of location parameters, u

	Duration (h)								
Region	**0.25**	**0.50**	**0.75**	**1.0**	**2.0**	**3.0**	**6.0**	**12.0**	**24.0**
N	73.322	53.709	42.127	34.669	19.737	13.983	7.634	4.187	2.599
Ne	41.517	29.925	24.277	20.247	11.811	8.428	4.595	2.521	1.891
C	53.001	38.899	31.044	25.924	14.887	10.575	5.822	3.063	2.291
E	102.589	68.096	51.422	40.647	22.455	15.323	8.032	4.142	2.831
W	71.187	48.265	37.516	30.637	18.011	13.146	7.012	3.716	2.242
S	88.878	66.004	52.866	44.025	26.202	19.098	10.658	6.182	4.403

Table 6 | IDF relationship of this study (extreme intensity in mm/h)

		Return period (years)								
D (h)	Region	2	5	10	25	50	100	200	500	1,000
0.25	North	85.2	121.8	146.1	176.8	199.5	222.1	244.6	274.3	296.7
	Northeast	54.3	93.7	119.7	152.7	177.1	201.4	225.6	257.5	281.6
	Central	68.1	114.9	145.9	185.1	214.2	243.0	271.7	309.6	338.3
	East	116.4	159.0	187.2	222.8	249.3	275.5	301.7	336.2	362.3
	West	81.8	114.4	136.1	163.4	183.7	203.8	223.9	250.3	270.3
	South	99.9	133.9	156.4	184.9	206.0	226.9	247.8	275.4	296.2
0.5	North	60.1	80.0	93.2	109.8	122.1	134.4	146.6	162.7	174.8
	Northeast	38.6	65.5	83.3	105.8	122.5	139.1	155.6	177.4	193.8
	Central	49.3	81.6	103.0	130.0	150.0	169.9	189.7	215.8	235.5
	East	76.2	101.1	117.7	138.5	154.0	169.4	184.7	205.0	220.2
	West	55.7	78.6	93.7	112.9	127.1	141.2	155.3	173.8	187.9
	South	73.4	96.4	111.6	130.9	145.1	159.3	173.4	192.0	206.1
0.75	North	47.4	63.7	74.5	88.1	98.3	108.3	118.3	131.5	141.5
	Northeast	31.5	53.8	68.6	87.3	101.2	114.9	128.6	146.7	160.4
	Central	39.4	65.3	82.5	104.1	120.2	136.1	152.0	173.0	188.8
	East	57.4	75.8	88.0	103.4	114.9	126.2	137.6	152.5	163.8
	West	43.2	60.9	72.7	87.5	98.5	109.4	120.2	134.6	145.4
	South	58.8	77.2	89.4	104.8	116.2	127.6	138.9	153.8	165.0
1	North	39.4	53.8	63.4	75.6	84.6	93.5	102.4	114.1	123.0
	Northeast	26.6	46.2	59.1	75.5	87.7	99.7	111.7	127.6	139.6
	Central	33.0	54.7	69.1	87.3	100.8	114.2	127.5	145.2	158.5
	East	45.7	61.3	71.6	84.7	94.3	104.0	113.5	126.2	135.7
	West	35.7	51.3	61.6	74.7	84.3	93.9	103.5	116.1	125.7
	South	49.1	64.9	75.3	88.4	98.2	107.9	117.6	130.3	139.9
2	North	22.3	30.4	35.8	42.5	47.5	52.5	57.5	64.0	69.0
	Northeast	15.8	28.2	36.4	46.8	54.5	62.2	69.8	79.8	87.4
	Central	18.9	31.2	39.4	49.7	57.4	65.0	72.5	82.5	90.1
	East	25.6	35.4	41.9	50.1	56.2	62.3	68.3	76.2	82.2
	West	21.3	31.5	38.2	46.8	53.1	59.4	65.6	73.9	80.1
	South	29.6	40.0	47.0	55.7	62.2	68.7	75.1	83.6	90.0
3	North	15.9	21.8	25.7	30.6	34.2	37.9	41.5	46.2	49.9
	Northeast	11.4	20.7	26.8	34.5	40.3	46.0	51.7	59.2	64.8
	Central	13.4	22.3	28.1	35.5	41.0	46.5	51.9	59.1	64.5
	East	17.8	25.5	30.5	36.9	41.7	46.4	51.1	57.3	62.0
	West	15.9	24.4	30.0	37.2	42.4	47.7	52.9	59.8	65.0
	South	21.6	29.2	34.3	40.7	45.5	50.2	54.9	61.1	65.8
6	North	8.7	11.8	13.9	16.6	18.6	20.5	22.5	25.0	27.0
	Northeast	6.3	11.6	15.1	19.6	22.9	26.2	29.4	33.7	37.0
	Central	7.4	12.3	15.6	19.7	22.7	25.7	28.7	32.7	35.7
	East	9.5	14.1	17.1	20.9	23.7	26.5	29.3	33.0	35.8
	West	8.8	14.2	17.8	22.3	25.7	29.1	32.4	36.8	40.1
	South	12.3	17.5	21.0	25.3	28.5	31.7	34.9	39.1	42.3
12	North	4.7	6.5	7.6	9.0	10.1	11.1	12.2	13.6	14.6
	Northeast	3.5	6.4	8.4	10.8	12.7	14.5	16.3	18.7	20.5
	Central	3.9	6.6	8.4	10.7	12.4	14.0	15.7	17.9	19.5
	East	4.9	7.4	9.0	11.0	12.5	14.0	15.5	17.5	19.0
	West	4.8	8.0	10.1	12.8	14.8	16.7	18.7	21.3	23.3
	South	7.2	10.4	12.6	15.3	17.3	19.2	21.2	23.8	25.8
24	North	2.9	4.0	4.7	5.5	6.2	6.8	7.5	8.3	9.0
	Northeast	2.5	4.3	5.4	6.9	8.0	9.1	10.2	11.7	12.8
	Central	2.8	4.3	5.3	6.6	7.6	8.5	9.4	10.7	11.6
	East	3.2	4.4	5.2	6.1	6.9	7.6	8.3	9.3	10.0
	West	2.9	5.0	6.4	8.1	9.4	10.7	11.9	13.6	14.9
	South	5.0	7.0	8.4	10.0	11.3	12.5	13.7	15.4	16.6

D, duration.

Table 7 | IDF relationship of the Central from RID's study (extreme intensity in mm/h)

	Return period (years)								
Duration (h)	**2**	**5**	**10**	**25**	**50**	**100**	**200**	**500**	**1,000**
0.25	96.3	127.4	148	173.9	193.3	212.6	231.4	256.6	275.5
0.5	72.6	92.6	105.9	122.6	135	147.4	159.7	175.8	188
0.75	56.8	72.2	82.5	95.4	105	114.5	124	136.5	145.9
1	48.4	62.4	71.7	83.5	92.2	100.8	109.4	120.8	129.3
2	28.4	37.8	44	51.8	57.6	63.4	69.1	76.7	82.4
3	20.6	27.3	31.9	37.7	42	46.3	50.6	56.2	60.4
6	11.4	15.6	18.4	22	24.6	27.3	29.9	33.3	35.9
12	6	8.5	10.2	12.3	13.9	15.4	17	19	20.6
24	3.4	5	6	7.3	8.3	9.3	10.3	11.5	12.5

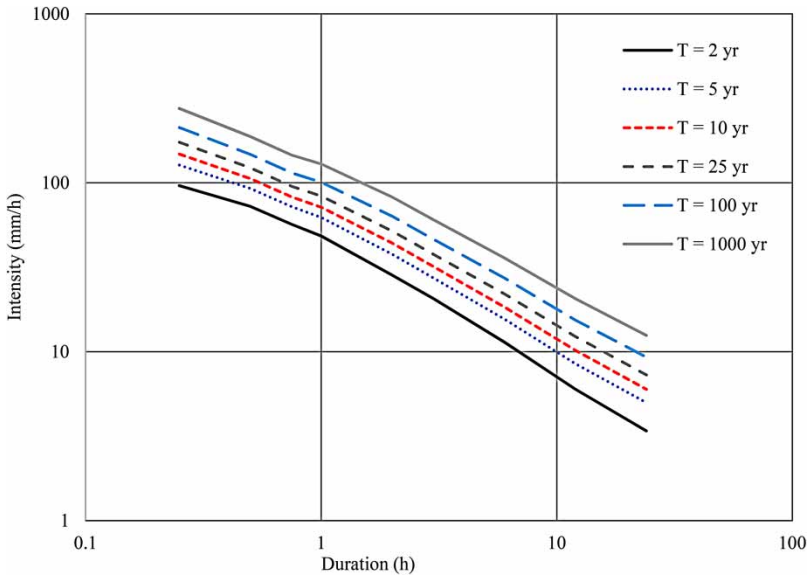

Figure 3 | IDF curve for the Central from this study.

They describe that the maximum intensity values from our study are all lower than those from RID for a 2-year return period; nonetheless, only a few for a 100-year return period at a higher duration are as shown in Figure 7.

Intensity ratios between this study and RID's values

It is always presumed that, due to climate change, the maximum rainfall intensity at a specific duration and the return period should progressively increase in accordance with time. Here we compare the rainfall intensities from two data sets: the older one from RID (1950–1998) to the more recent one in this study (1990–2016) (Table 1). These two data sets, even with some overlap, exhibit a range of time difference about 15–25 years. Therefore, the rainfall intensity values from this study should likely be higher than those from the RID study due to climate change. The rainfall intensity ratios of this study compared to the RID study are used to determine their change. If the ratio is higher than 1, it means the intensity is increasing as expected and vice versa. The intensity ratios of the North, Northeast, Central, East, West, and South are illustrated in Table 8, and the statistical summary of the intensity ratio is shown in Table 9.

Each region comprises 81 ratios, as the combination of nine durations and nine return periods is taken into account. The ratios that are higher than 1.0 show the increase in rainfall intensity from the past to the present. The statistical summary in Table 9 shows that the highest number of the higher-than-1 ratio is in the East region for 34 ratios and the lowest in the

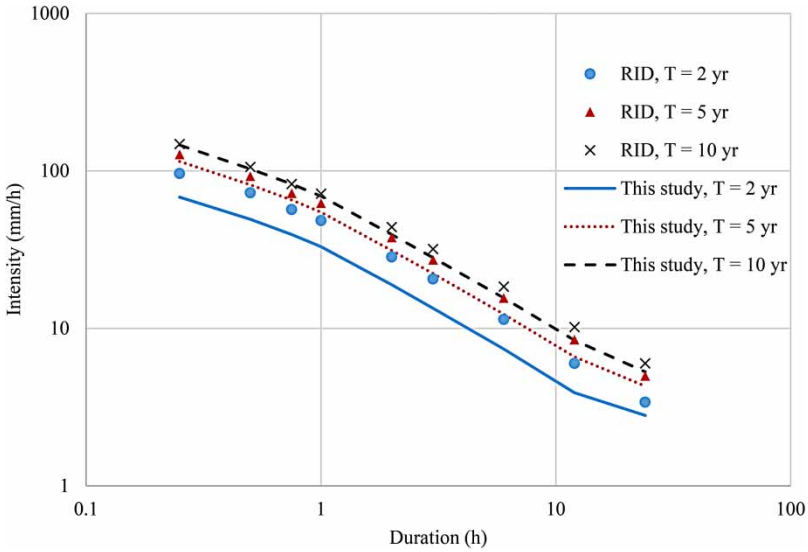

Figure 4 | IDF curves comparison between those from the RID study and this study for the Central region at return periods of 2, 5 and 10 years.

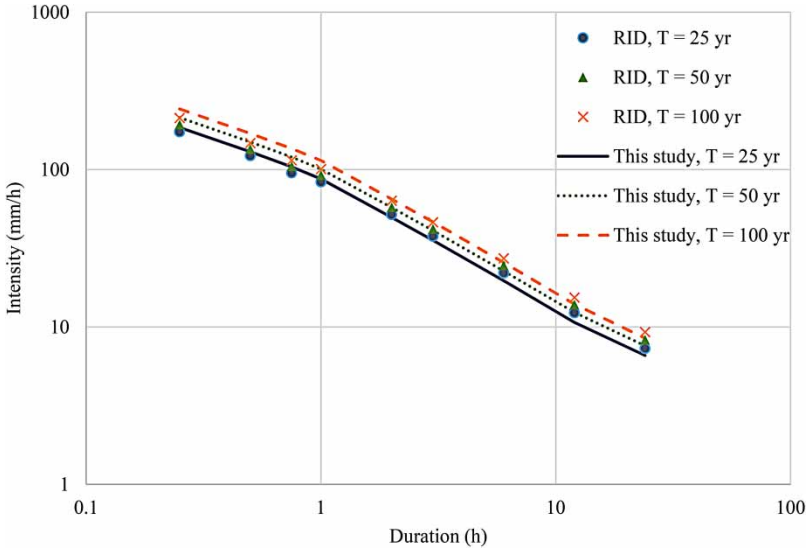

Figure 5 | IDF curves comparison between those from the RID study and this study for the Central region at return periods of 25, 50 and 100 years.

Northeast at 2 ratios. Considering the mean values of ratio and numbers of higher-than-1 ratio (Table 9), we can classify all regions into three groups, (1) Northeast, (Ne), (2) North, West, and South (NWS), and (3) Central and East (CE). The Northeast group (Ne) consists of a single region called the Khorat plateau. Its landscape is undulating terrain with a range of Phu Phan dividing the region into two basins, i.e., the Sakon Nakhon Basin in the North and the Khorat Basin in the South. A majority of the region drains its into the Mekong River. The second group consisting of the NWS is mountainous with mountain ranges lying along the north-south direction extending from southernmost to northernmost. The rainfall of the area derives mainly from the Southwest monsoon and it always causes flash floods and landslides. The last group, CE, is the combination of the Central lowland and the low hilly eastern part. Most of the drainage from this region goes to the Gulf of Thailand.

The plateau, the Northeast group, has two greater-than-1 ratios at 0.25 h duration for 500- and 1,000-year return periods with the mean intensity value of 0.81 (Tables 8 and 9). The mountainous regions, the NWS, have the greater-than-1 ratios of 8, 6, and 7, with the mean intensity values of 0.89, 0.90, and 0.90 for the North, the West, and the South, respectively. The ratios for the

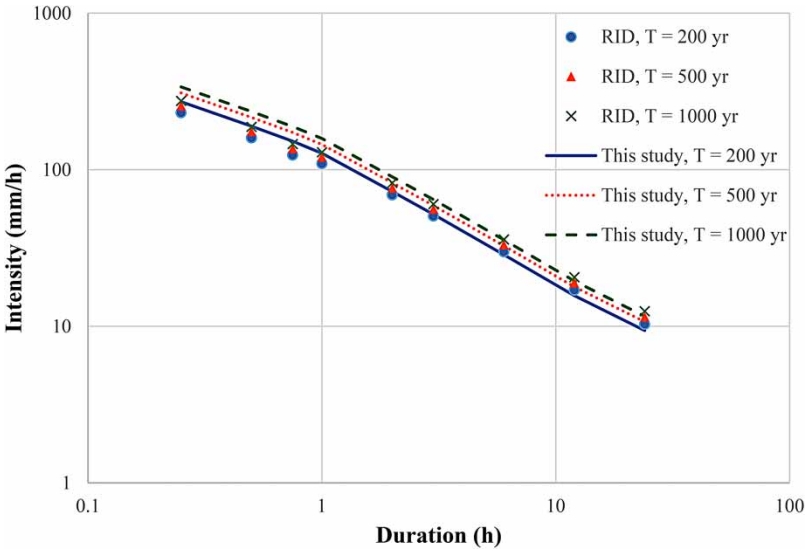

Figure 6 | IDF curves comparison between those from the RID study and this study for the Central region at return periods of 200, 500 and 1,000 years.

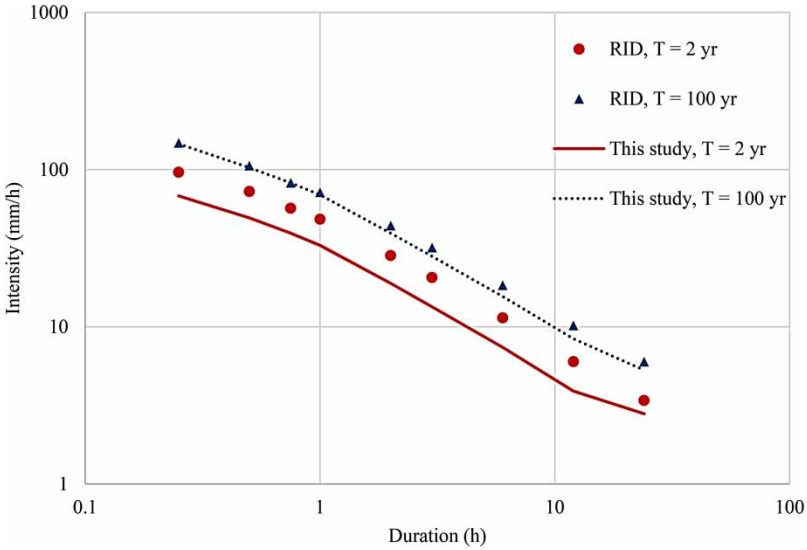

Figure 7 | IDF curves comparison between those from the RID study and this study for the Central region at return periods of 2 and 100 years.

North and the South are only from the smallest duration, 0.25 h. The North has eight ratios at 5-, 10-, 25-, 50-, 100-, 500-, and 1,000-year return periods, while the South has seven ratios from 10- to 1,000-year return periods. The West region, which is located between the North and the South, has six ratios with five from the smallest duration of 0.25 h and the return periods between 50 and 1,000 years as well as one ratio from the next smallest duration of 0.5 h with return periods of 1,000 years.

The last groups, which are the Central and the East, have 31 and 34 ratios, respectively (Tables 8 and 9). For the Central region, the number of greater-than-1 ratios is four each from the 25- and 50-year return periods with the durations of 0.25, 0.5, 0.75, and 1 h; five ratios from the 100-year return period with the durations of 0.25–2 h; and six ratios each for the return periods of 200, 500, and 1,000 years with the durations of 0.25–3 h (Table 8).

The East region has the largest number of 34 ratios with irregular distribution. There are nine ratios each of 0.25 and 0.5 h durations for all return periods, that is, one ratio of 2-year return period for 0.75 durations, 4 each of 3 and 12 h durations for 100- to 1,000-year return periods, and seven ratios of 6 h duration for 10- to 1,000-year return periods (Table 8). The analysis of the Eastern region in this study, however, was the least reliable because only three data sets were used.

Table 8 | Intensity ratios of this study to RID's values (bold values show greater-than-1 ratios)

Return Period (years)	Region	Duration (h)								
		0.25	0.5	0.75	1	2	3	6	12	24
2	N	0.95	0.90	0.89	0.89	0.88	0.87	0.86	0.83	0.89
	Ne	0.53	0.52	0.52	0.53	0.52	0.52	0.52	0.50	0.60
	C	0.71	0.68	0.69	0.68	0.66	0.65	0.65	0.66	0.82
	E	**1.18**	**1.07**	**1.01**	0.98	0.95	0.95	0.93	0.91	1.00
	W	0.82	0.76	0.74	0.74	0.77	0.79	0.76	0.74	0.75
	S	0.95	0.91	0.91	0.90	0.89	0.88	0.85	0.83	0.87
5	N	**1.05**	0.91	0.90	0.92	0.87	0.84	0.83	0.80	0.85
	Ne	0.71	0.68	0.68	0.70	0.68	0.68	0.66	0.65	0.73
	C	0.90	0.88	0.90	0.88	0.83	0.82	0.79	0.78	0.86
	E	**1.17**	**1.07**	1.00	0.98	0.96	0.98	0.99	0.96	0.97
	W	0.91	0.85	0.81	0.82	0.83	0.87	0.84	0.82	0.85
	S	0.99	0.93	0.92	0.91	0.90	0.89	0.85	0.82	0.83
10	N	**1.09**	0.90	0.91	0.93	0.87	0.83	0.82	0.77	0.82
	Ne	0.80	0.75	0.75	0.77	0.74	0.74	0.73	0.70	0.79
	C	0.99	0.97	1.00	0.96	0.90	0.88	0.85	0.83	0.89
	E	**1.16**	**1.07**	1.00	0.97	0.96	0.99	**1.01**	0.97	0.92
	W	0.95	0.89	0.84	0.85	0.86	0.90	0.87	0.85	0.87
	S	**1.01**	0.94	0.92	0.92	0.91	0.89	0.85	0.82	0.81
25	N	**1.15**	0.92	0.90	0.94	0.86	0.83	0.81	0.76	0.80
	Ne	0.88	0.82	0.82	0.84	0.80	0.79	0.78	0.75	0.84
	C	**1.06**	**1.06**	**1.09**	**1.05**	0.96	0.94	0.89	0.87	0.90
	E	**1.16**	**1.07**	0.99	0.97	0.95	1.00	**1.03**	0.99	0.93
	W	0.99	0.93	0.87	0.89	0.80	0.92	0.90	0.87	0.90
	S	**1.03**	0.98	0.93	0.93	0.91	0.89	0.85	0.81	0.80
50	N	**1.16**	0.92	0.91	0.94	0.86	0.82	0.80	0.75	0.79
	Ne	0.92	0.86	0.86	0.88	0.83	0.83	0.81	0.78	0.86
	C	**1.11**	**1.11**	**1.14**	**1.09**	1.00	0.98	0.92	0.89	0.91
	E	**1.15**	**1.07**	0.99	0.97	0.96	1.00	**1.04**	1.00	0.92
	W	**1.01**	0.95	0.88	0.90	0.89	0.94	0.92	0.86	0.91
	S	**1.04**	0.95	0.93	0.94	0.91	0.90	0.85	0.81	0.79
100	N	**1.18**	0.93	0.92	0.95	0.86	0.82	0.80	0.74	0.79
	Ne	0.96	0.89	0.90	0.92	0.86	0.85	0.84	0.80	0.89
	C	**1.14**	**1.15**	**1.19**	**1.13**	**1.02**	1.00	0.94	0.91	0.91
	E	**1.15**	**1.07**	0.99	0.97	0.96	**1.01**	**1.05**	**1.01**	0.92
	W	**1.03**	0.97	0.90	0.92	0.90	0.95	0.93	0.90	0.92
	S	**1.05**	0.95	0.93	0.94	0.93	0.90	0.85	0.81	0.78
200	N	**1.19**	0.95	0.92	0.95	0.86	0.81	0.80	0.74	0.78
	Ne	0.99	0.92	0.92	0.94	0.88	0.87	0.85	0.82	0.91
	C	**1.17**	**1.19**	**1.23**	**1.17**	**1.05**	**1.03**	0.96	0.92	0.92
	E	**1.15**	**1.07**	0.99	0.96	0.96	**1.01**	**1.05**	**1.02**	0.90
	W	**1.04**	0.98	0.91	0.93	0.91	0.96	0.93	0.91	0.93
	S	**1.06**	0.96	0.93	0.94	0.92	0.90	0.85	0.81	0.78
500	N	**1.21**	0.93	0.92	0.95	0.86	0.81	0.79	0.73	0.77
	Ne	**1.03**	0.95	0.95	0.97	0.90	0.89	0.88	0.84	0.93
	C	**1.21**	**1.23**	**1.27**	**1.20**	**1.08**	**1.05**	0.98	0.94	0.93
	E	**1.15**	**1.06**	0.99	0.96	0.96	**1.02**	**1.06**	**1.02**	0.90
	W	**1.06**	1.00	0.92	0.95	0.92	0.98	0.94	0.91	0.94
	S	**1.07**	0.96	0.93	0.95	0.92	0.90	0.85	0.81	0.78
1,000	N	**1.22**	0.93	0.93	0.96	0.86	0.81	0.79	0.73	0.77
	Ne	**1.05**	0.97	0.97	0.99	0.92	0.90	0.88	0.85	0.94
	C	**1.23**	**1.25**	**1.29**	**1.23**	**1.09**	**1.07**	0.99	0.95	0.93
	E	**1.15**	**1.07**	0.99	0.96	0.96	**1.02**	**1.07**	**1.02**	0.90
	W	**1.07**	**1.01**	0.93	0.95	0.93	0.98	0.95	0.92	0.95
	S	**1.07**	0.96	0.93	0.95	0.92	0.90	0.85	0.81	0.77

Table 9 | Statistical summary of intensity ratios

Region	No. of ratio > 1	Mean	SD	Min.	Max.
N	8	0.89	0.1099	0.73	1.22
Ne	2	0.81	0.1329	0.50	1.05
C	31	0.98	0.1611	0.65	1.29
E	34	1.01	0.0683	0.90	1.18
W	6	0.90	0.0734	0.74	1.07
S	7	0.90	0.0704	0.77	1.07

Table 10 | Comparison of rainfall intensities of IDF studies from Weesakul *et al.* (2017) and Shrestha *et al.* (2017)

Publication		Weesakul *et al.* (2017)			Shrestha *et al.* (2017)		
T (years)	D (h)	BP 1990–2014	FP 2015–2039	R	BP 1981–2010	FP 2011–2030	R
2	1	51.5	92.0	1.8	37.6	41.4	1.1
	3	21.5	30.0	1.4	31.2	33.0	1.1
	6	10.0	16.5	1.5	14.8	18.3	1.2
	12	5.5	8.1	1.5	8.3	8.7	1.0
	24	3.2	4.7	1.5	4.8	5.0	1.0
5	1	60.8	93.0	1.5	47.2	48.8	1.0
	3	28.8	39.3	1.4	38.6	43.6	1.1
	6	15.5	21.1	1.4	20.4	25.4	1.2
	12	8.0	10.2	1.3	10.6	13.3	1.3
	24	4.5	6.2	1.4	6.0	6.9	1.2

T, return periods (years); D, durations (h); BP, base period; FP, future period; R, ratio of FP to BP.

For the practical planning and design of hydraulic infrastructures, we have to choose appropriate rainfall intensity from IDF curves by first considering rainfall duration and then return period. Rainfall duration is chosen from the size and shape of the watershed or from its time of concentration, while a small watershed normally gives a shorter duration (Chow *et al.* 1988). The choice of return period depends on the size of watershed and the risk of failure (Chow *et al.* 1988).

Extreme outflow discharge from a small watershed does not always cause serious damage compared to that from a large watershed. Table 8 shows that the greater-than-1 ratios mostly exist at short durations especially at higher return periods. At return periods of 500 and 1,000 years, the greater-than-1 ratios exist at 15 min for all groups. For lower return periods at 50, 100, and 200 years, the ratios exist at 15 min for all except group 1 (Ne). The planning and design of hydraulic structures of larger watersheds with longer rainfall durations and involving higher risk require longer return periods. Therefore, the findings presented in Table 8 imply the acceptability of the national standard IDF curves from RID for all of Thailand. However, for the last group, namely the East and the Central regions, at the return periods from 50 years onward, the planning and design of hydraulic structures should be conducted with care.

Table 9 summarizes the number of greater-than-1 ratios for all regions which are classified into three groups, i.e., Ne, NWS, and CE. The first group, Ne, comprises only two greater-than-1 ratios from 81 ratios. The NWS group shows average greater-than-1 ratios of 7.3. Regarding the CE group, its average number of greater-than-1 ratios is 34.5 from 81 ratios. These results suggest that Thailand's IDF curves that were derived from the accurate historical rainfall data can render reliable design storms. To confirm this finding, two independent studies of IDF curves of the same rainfall station in Bangkok, Thailand, were investigated.

Weesakul *et al.* (2017) and Shrestha *et al.* (2017) studied future IDF curves from the same data set but with different methodology. The former assumed the annual maximum intensity series following Gumbel (EV 1) distribution, while the latter assumed the general extreme value (EV3) distribution. The former acquired the future precipitation time series during 2015–2039 from a global climate model using the GEM 2-ES model with the greenhouse gas scenario of RCP4.5, whereas

the latter derived the future ones during 2011–2030 from eight models with the scenario of SRA1B. The two scenarios are similar in the greenhouse gas of low to medium concentration. For bias correction, the former used the current data sets of 1990–2014, while the latter used those of 1981–2010.

The values of extreme rainfall intensities in Table 10 were digitized from Weesakul *et al.* (2017) and Shrestha *et al.* (2017). The two studies used the same rainfall data set from the Sukhumvit area in Bangkok. The base periods (BP) and the forecast periods (FP) of the two studies are somewhat similar (Table 10). The significant difference between both studies is that the latter used eight global climatic models, while the former used only one to generate the future daily rainfall data sets. The results of the latter, therefore, should be more reliable. When considering the ratios of FP intensities to BP intensities, the former values are between 1.3 and 1.8 with the mean of 1.47 and the latter values are in the range of 1.0–1.3 averaging at 1.12. This implies that the more reliable method renders the closer of the future values to the base values, even though larger-than-1 ratios present in all of the results. All climatic models assume an increase in greenhouse gas which may trigger higher rainfall intensity in the future. We cannot predict the long-term rate of the greenhouse gas emission. The COVID-19 pandemic is one recent example that can temporarily reduce the emission rate. Some studies and attempts have been implemented to reduce and stabilize the emission rate such as the green new deal energy plan and the like (Jacobson *et al.* 2019; Nielsen *et al.* 2020). This study, therefore, suggests that using an accurate historical data set could be favorable to that using lengthy synthesized future data set for generating the IDF relationships.

CONCLUSIONS

An accurate IDF curve is crucial for hydraulic infrastructure design. The accuracy of an IDF curve is not known beforehand because the historical set of precipitation data were used to predict the future rainfall information. Due to climate change, new IDF curves are expected to change as a result of increasing rainfall intensities. We have compared a set of past IDF curves (RID's study) with that of the recent ones (this study) and found that the majority of them did not increase as expected. Another shortcoming of this finding is the relatively small time-lapse of about 15–20 years between the two data sets from the RID study and this study.

ACKNOWLEDGEMENT

This research was funded by the College of Industrial Technology, King Mongkut's University of Technology North Bangkok (Grant No. Res-CIT0270/2021).

DATA AVAILABILITY STATEMENT

All relevant data are included in the paper or its Supplementary Information.

REFERENCES

AghaKouchak, A., Ragno, E., Love, C. & Moftakhari, H. 2018 *Projected Changes in California's Precipitation Intensity-Duration-Frequency Curves*. Report California Energy Commission, California, USA.

Agilan, V. & Umamahesh, N. V. 2016 Is the covariate based non-stationary rainfall IDF curve capable of encompassing future rainfall changes? *Journal of Hydrology* **541** (B), 1441–1455.

Balbastre-Soldevila, R., Garcia-Bartual, R. & Andrea-Domenech, I. 2019 A comparison of design storms for urban drainage system applications. *Water* **11**, 757.

Bellprat, O., Guemas, V., Doblas-Reyes, F. & Donat, M. G. 2019 Towards reliable extreme weather and climate event attribution. *Nature Communications* **10**, 1732.

Bernard, M. M. 1932 Formulas for rainfall intensities of long durations. *Transactions of the American Society of Civil Engineers* **96**, 592–624.

Bezak, N., Sraj, M., Rusjan, S. & Mikos, M. 2018 Impact of the rainfall duration and temporal rainfall distribution defined using the Huff curves on the hydraulic flood modelling results. *Geosciences* **8**, 69.

Buchanan, M. 2020 The limit of a model. *Nature Physics* **16**, 605.

Bumpenkit, P. 1999 *The Relationship of Rainfall Intensity Duration Frequency of Difference Regions in Thailand*. Report Royal Irrigation Department (RID), Thailand.

Cheng, L. & AghaKouchak, A. 2014 Nonstationary precipitation intensity-duration-frequency curves for infrastructure design in a changing climate. *Scientific Reports* **4**, 7093.

Choi, J., Lee, O., Jang, J., Jang, S. & Kim, S. 2019 Future intensity-depth-frequency curves estimation in Korea under representative concentration pathway scenarios of Fifth assessment report using scale-invariance method. *International Journal of Climatology* **39**, 887–900.

Chokkavarapu, N. & Mandla, V. R. 2019 Comparative study of GCMs, RCMs, downscaling and hydrological models: a review toward future climate change impact estimation. *SN Applied Sciences* **1**, 1698.

Chow, V. T., Maidment, D. R. & Mays, L. W. 1988 *Applied Hydrology*. McGraw-Hill, New York, USA.

Cook, L. M., McGinnis, S. & Samaras, C. 2020 The effect of modelling choices on updating intensity-duration-frequency curves and stormwater infrastructure designs for climate change. *Climatic Change* **159**, 289–308.

da Silva, L. V., Casaroli, D., Evangelista, A. W. P., Junior, J. A. & Battisti, R. 2019 Rainfall intensity-duration-frequency relationships for risk analysis in the region of Matopiba, Brazil. *Revista Brasileira de Meteorologia* **34** (2), 247–254.

Ganguli, P. & Coulibaly, P. 2017 Does nonstationary in rainfall require nonstationary intensity-duration-frequency curves? *Hydrology and Earth System Sciences* **21**, 6461–6483.

Ganguli, P. & Coulibaly, P. 2019 Assessment of future changes in intensity-duration-frequency curves for Southern Ontario using North American (NA)-CORDEX models with nonstationary methods. *Journal of Hydrology: Regional Studies* **22**, 100587.

Hershfield, D. 1962 Extreme rainfall relationships. *ASCE Journal of the Hydraulics Division* 88, 73–92.

Hu, H. & Ayub, B. M. 2019 Machine learning for projecting extreme precipitation intensity for short durations in a changing climate. *Geosciences* **9**, 209.

Jacobson, M. Z., Delucchi, M. A., Cameron, M. A., Coughlin, S. J., Hay, C. A., Manogaran, I. P., Shu, Y. & von Krauland, A.-K. 2019 Impacts of green new deal energy plans on grid stability, cost, jops, health, and climate in 143 countries. *One Earth* **1**, 449–463.

Kohnova, S., Foldes, G., Labat, M. M. & Hlavcova, K. 2019 Changes in the IDF curves of short-term rainfall in the mountainous and lowland areas of Slovakia. *Earth and Environmental Science* **362**, 012083.

Koutsoyiannis, D., Kozonis, D. & Manetas, A. 1998 A mathematical framework for studying rainfall intensity-duration-frequency relationships. *Journal of Hydrology* **206**, 118–135.

Liew, S. C., Raghavan, S. V. & Liong, S.-Y. 2013 How to construct future IDF curves, under changing climate, for sites with scare rainfall records? *Hydrological Processes* **28** (8), 3276–3287.

Martin, S. A. & Riichie, R. J. 2020 Sourcing Thai geography literature for ASEAN and international education. *Singapore Journal of Tropical Geography* **41** (1), 61–85.

Mirhosseini, G., Srivastava, P. & Stefanova, L. 2012 The impact of climate change on rainfall intensity-duration-frequency (IDF) curves in Alabama. *Regional Environment Change*. doi:10.1007s10113-012-0375-5.

Moriondo, M. & Bindi, M. 2006 Comparison of temperature simulated by GCMs, RCMs and statistical downscaling: potential application in studies of future crop development. *Climate Research* **30** (2), 149–160.

Mustonen, S. E. 1969 *Rainfall-Intensity-Frequency Curves for Some Stations in Thailand*. Thai Meteorological Department, Bangkok, Thailand.

Nielsen, K. S., Stern, P. C., Dietz, T., Gilligan, J. M., van Vuuren, D. P., Figueroa, M. J., Folke, C., Gwozdz, W., Ivanova, D., Reisch, L. A., Vandenbergh, M. P., Wolske, K. S. & Wood, R. 2020 Improving climate change mitigation analysis: a framework for examining feasibility. *One Earth* **3**, 325–336.

Noor, M., Ismail, T., Chung, E.-S., Shahid, S. & Sung, J. H. 2018 Uncertainty in rainfall intensity duration frequency curves of Peninsular Malaysia under changing climate scenarios. *Water* **10**, 1750.

Shepherd, T. G., Boyd, E., Calel, R. A., Chapman, S. C., Dessai, S., Dima-West, I. M., Fowler, H. J., James, R., Maraun, D., Martius, O., Senior, C. A., Sobel, A. H., Stainforth, D. A., Tett, S. F. B., Trenberth, K. E., van den Hurk, B. J. J. M., Watkins, N. W., Wilby, R. L. & Zenghelis, D. A. 2018 Storylines: an alternative approach to representing uncertainty in physical aspects of climate change. *Climatic Change* **151**, 555–571.

Sherman, C. W. 1931 Frequency and intensity of excessive rainfall at Boston. *Transactions of the American Society of Civil Engineering* **95**, 951–960.

Shrestha, A., Babel, M. S., Weesakul, S. & Vojinovic, Z. 2017 Developing intensity-duration-frequency (IDF) curve under climate change uncertainty: the case of Bangkok, Thailand. *Water* **9**, 145.

Sillmann, J., Shepherd, T. G., van den Hurk, B., Hazeleger, W., Martius, O., Slingo, J. & Zscheischler, J. 2021 Event-based storylines to address climate risk. *Earth's Future* **9**, e2020EF001783.

Sun, Y., Wendi, D., Kim, D. E. & Liong, S.-Y. 2019 Deriving intensity-duration-frequency (IDF) curves using downscaled in situ rainfall assimilated with remote sensing data. *Geoscience Letters* **6**, 17.

Thompson, E. L. & Smith, L. A. 2019 Escape from model-land. *Economics* **13**, 40.

Trenberth, K. E. 2011 Changes in precipitation with climate change. *Climate Research* **47** (1), 123–138.

Weesakul, U., Chaowiwat, W., Rehan, M. M. & Weesakul, S. 2017 Modification of a design storm pattern for urban drainage systems considering the impact of climate change. *Engineering and Applied Science Research* **44** (3), 161–169.

White, P., Hilario, F. D., Guzman, R. G. & Cinco, T. A. 2009 *A Review of Climate Change Model Predictions and Scenario Selection for Impacts on Asian Aquaculture*. PAGASA, Philippine.

Wilby, R. L., Dawson, C. W. & Barrow, E. M. 2002 SDMS – a decision support tool for the assessment of regional climate change impacts. *Environmental Modeling and Software* **17** (2), 17–159.

Woo, G. & Johnson, N. F. 2018 Stochastic modelling of possible pasts to illuminate future risk. In: *Oxford Handbook of Complex Disaster Risks* (Shultz, J., Rechkemmer, A. & Johnson, N. F., eds). Oxford University Press, UK.

First received 23 June 2021; accepted in revised form 8 September 2021. Available online 24 September 2021